Supplementary Information

Dry chemical method for dispersing Ir nanoparticles in the pores of activated carbon and their X-ray absorption spectroscopy analysis

Hiroyuki Itoi,[†] *Takashi Tachikawa,*[§] *Ryutaro Suzuki,*[†] *Hideyuki Hasegawa,*[†] *Hiroyuki Iwata,*[‡] *Yoshimi Ohzawa,*[†] *Atsushi Beniya*[§] *and Shougo Higashi* *[§]

[†]Department of Applied Chemistry, and [‡]Department of Electrical and Electronics Engineering, Aichi Institute of Technology, Yachigusa 1247, Yakusa-cho, Toyota, 470-0392, Japan.

[§]Frontier Research-Domain, Toyota Central R&D Labs., Inc., Yokomichi 41-1, Nagakute, 480-1192, Japan.

*E-mail: itoi-hiroyuki@aitech.ac.jp, shigashi@mosk.tytlabs.co.jp

Supplementary note 1 | Materials and synthesis

(1,5-Cyclooctadiene)-η^5-indenyl)iridium (I) (IrIndCOD) was purchased from Sigma-Aldrich. IrIndCOD and activated carbon (AC, Kansai Coke and Chemicals Co., Ltd) were used as received. AC was dried in a glass ampoule at 150 ºC for 6 h under vacuum. The amount of the dried AC was calculated from the weight difference between the empty ampoule and the ampoule containing dried AC. IrIndCOD was precisely weighed using a microbalance so that the AC/Ir weight ratios were 99.5:0.5, 98:2, 97:3, 95:5, and 90:10. Next, IrIndCOD and a magnetic stir bar were introduced into the glass ampoule, which was then sealed under vacuum. For the adsorption of IrIndCOD in AC, the glass ampoule was heated at a ramp rate of 1 ºC min^{-1} up to 100 ºC and kept at this temperature for 24 h with stirring. The glass ampoule was finally heated in a muffle furnace at 400 ºC for 3 h to decompose the adsorbed IrIndCOD.

Supplementary note 2 | Measurements

X-ray diffraction (XRD) patterns were collected using an XRD-6100 instrument (Shimadzu) with Cu Kα radiation (λ = 1.5418 Å), at an accelerating voltage of 30 kV and a current of 20 mA. Nitrogen adsorption/desorption measurements were performed with ASAP2020 at −196 ºC. AC was dried at 150 ºC for 6 h under vacuum before measurement. The Brunauer–Emmett–Teller specific surface area (BET SSA) was calculated using the adsorption isotherm at P/P_0 = 0.05–0.20. The total pore volume (V_{total}) was determined from the adsorbed amount at P/P_0 = 0.96. The micropore volume (V_{micro}) was estimated using the Dubinin–Radushkevich method. The mesopore volume (V_{meso}) was calculated by subtracting the micropore volume from the total pore volume ($V_{meso} = V_{total} - V_{micro}$). Pore size distribution was calculated using density functional theory. Transmittance electron microscope (TEM) observation was conducted with a JEM-2100Plus (JEOL) at an accelerating voltage of 200 kV. X-ray photoelectron spectroscopy (XPS) analysis was performed with a KRATOS ESCA-3400 instrument using Mg Kα radiation (1253.6 eV). Scanning electron microscopy (SEM) images were collected with a Superscan SS-550 (Shimadzu) at an accelerating voltage of 15 kV.

Supplementary note 3 | BET SSA, pore volumes, and pore size distribution of AC

Nitrogen adsorption/desorption measurement was conducted with a Micrometrics ASAP 2020 apparatus at −196 ºC. Prior to the analysis, AC was dried at 150 ºC for 6 h under vacuum. The AC/Ir samples were treated under N_2 atmosphere before measurement to prevent the adsorption of H_2O. The Brunauer–Emmett–Teller specific surface area (BET SSA) was determined using the adsorption isotherm at P/P_0 = 0.05–0.20. The total pore volume (V_{total}) was calculated from the adsorption amount at P/P_0 = 0.96. The micropore volume (V_{micro}) was estimated by the Dubinin-Radushkevich method. The mesopore volume (V_{meso}) was calculated by subtracting the micropore volume from the total pore volume ($V_{meso} = V_{total} - V_{micro}$). Fig S1a shows the nitrogen adsorption/desorption isotherms for AC. The BET SSA of AC was determined to be 3160 $m^2\ g^{-1}$. The micro, meso, and total pore volumes of AC were calculated to be 0.99, 0.60, and 1.59 $cm^3\ g^{-1}$, respectively. As shown in the pore size distribution of AC (Fig. S1b), AC has pores less than 4 nm in size. The AC/Ir samples show the decrease of both micro- and mesopore volumes by the Ir loading (Fig. S1b), indicating that the Ir nanoparticles are supported not only in the micropores but also in the mesopores, irrespective of the amount of Ir.

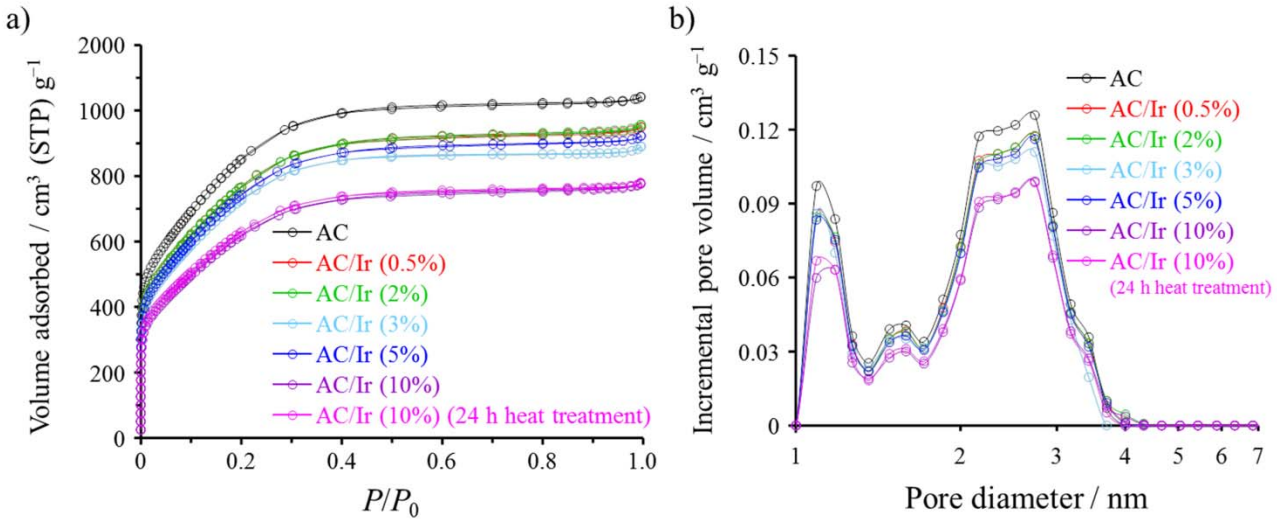

Fig. S1 Results of nitrogen adsorption/desorption measurements of AC.

Table S1 The BET SSAs and pore volumes for AC/Ir samples and AC.

sample	BET SSA ($m^2\ g^{-1}$)	V_{total} ($cm^3\ g^{-1}$)	V_{micro} ($cm^3\ g^{-1}$)	V_{meso} ($cm^3\ g^{-1}$)
AC	3160	1.59	0.99	0.60
AC/Ir (0.5%)	2850	1.44	0.88	0.56
AC/Ir (2%)	2850	1.45	0.88	0.57
AC/Ir (3%)	2710	1.35	0.84	0.51
AC/Ir (5%)	2770	1.40	0.56	0.55
AC/Ir (10%)	2310	1.18	0.75	0.43
AC/Ir (10%)[a]	2350	1.19	0.72	0.46

[a] Heat treated at 400 ºC for 24 h.

Supplementary note 4 | Estimation of molar ratio from XANES spectra

The Ir L_3 edge X-ray absorption spectroscopy (XAS) data were collected on the BL11S line at the Aichi Synchrotron Radiation Center. The beamline has an energy range of 5 keV – 25 keV for spectroscopy. XAS spectra of the samples and a Pt foil were measured simultaneously in transmission geometry. We used the XAS spectra of the Pt foil as a reference and analyzed the obtained X-ray absorption near edge structure (XANES) spectra using Athena.[1]

We calculated the XAS spectra ($\mu(E)$) from the incident (I_0(E)) and transmitted (I_1(E)) X-ray intensities using the following equation:

$$I_1(\mathrm{E}) = I_0(E)\exp\big(-\mu(E)\big) \qquad (1)$$

In this study, the absorption spectra were normalized so as to make the difference between the regression equations of the pre-edge ($E < E_0$, E_0 is the energy at the absorption edge) and post-edge ($E > E_0$) unity at E_0. The regression equations for the pre-edge are linear equations and those for the post-edge are third order polynomials. We plotted the normalized absorption spectra (we denote this normalized spectra as $\mu^{\mathrm{norm}}(E)$) in the range of 11.20 to 11.25 keV as the XANES spectra as shown in Fig. 4.

If the AC/Ir samples consisted of IrO_2, Ir, and IrIndCOD, as we consider in this study, the absorption spectra should be expressed as follows;

$$\mu^{\mathrm{norm}}(E) = \mathrm{a}\mu^{\mathrm{norm}}_{\mathrm{IrO2}}(E) + \mathrm{b}\mu^{\mathrm{norm}}_{\mathrm{Ir}}(E) + \mathrm{c}\mu^{\mathrm{norm}}_{\mathrm{IrIndCOD}}(E) \qquad (2)$$

where a, b and c are the molar ratios of each of the constituents. This means that the ratio used for linear combination fitting using each control sample is equal to the molar ratio of each constituent.

As we show in Fig. 4, the $\mu^{\mathrm{norm}}(E)$ for all five samples were well-fitted with a linear combination of each normalized XAS spectra for the control samples of IrO_2, Ir and IrIndCOD, corresponding to$\mu^{\mathrm{norm}}_{\mathrm{IrO2}}(E)$, $\mu^{\mathrm{norm}}_{\mathrm{Ir}}(E)$ and $\mu^{\mathrm{norm}}_{\mathrm{IrIndCOD}}(E)$, respectively.

Supplementary note 5 | Comparison of R-factor for XAS spectra obtained assuming with and without IrIndCOD for AC/Ir (0.5%)

In Fig. S2, we compared the R-factors of the XANES spectra obtained with and without IrIndCOD for AC/Ir (0.5%). In both cases, we see a good agreement between the experimental and fitting results (linear combination ratios and R-factors are summarized in Table S2), suggesting that the amount of IrIndCOD in AC/Ir (0.5%) is negligible.

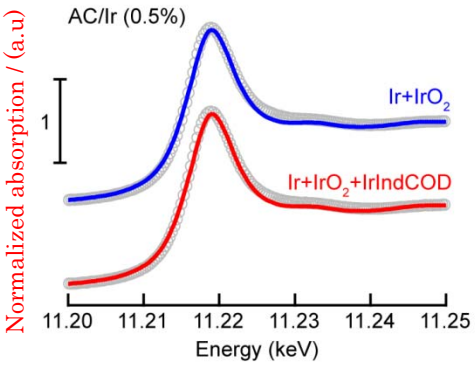

Fig. S2 XANES spectra of AC/Ir (0.5%) and best fitted curves using IrO_2 and Ir spectra without IrIndCOD and with IrIndCOD spectra. Solid lines are simulated XANES spectra.

Table S2 Comparison of the R-factor for XAS spectra for AC/Ir (0.5%) with different models with IrIndCOD and without IrIndCOD.

Model	IrO_2 : Ir : IrIndCOD	R-factor
IrO_2 + Ir + IrIndCOD	0.464 ± 0.012 : 0.482 ± 0.012 : 0.054 ± 0.024	0.0037
IrO_2 + Ir	0.491 ± 0.015 : 0.509 ± 0.009	0.0040

Supplementary note 6| TEM images of AC/Ir (10%) after the different heat treatment conditions

We examined the heat treatment of AC/IrIndCOD (10%) by changing the heat treatment conditions. Fig. S3 and S4 show the TEM images of the AC/IrIndCOD (10%) after the heat treatment at 400 ºC for 24 h and 500 ºC for 3 h, respectively. Both samples contain more nanoparticles when compared with AC/Ir (10%) (Fig. 3d), which was subject to the heat treatment at 400 °C for 3 h.

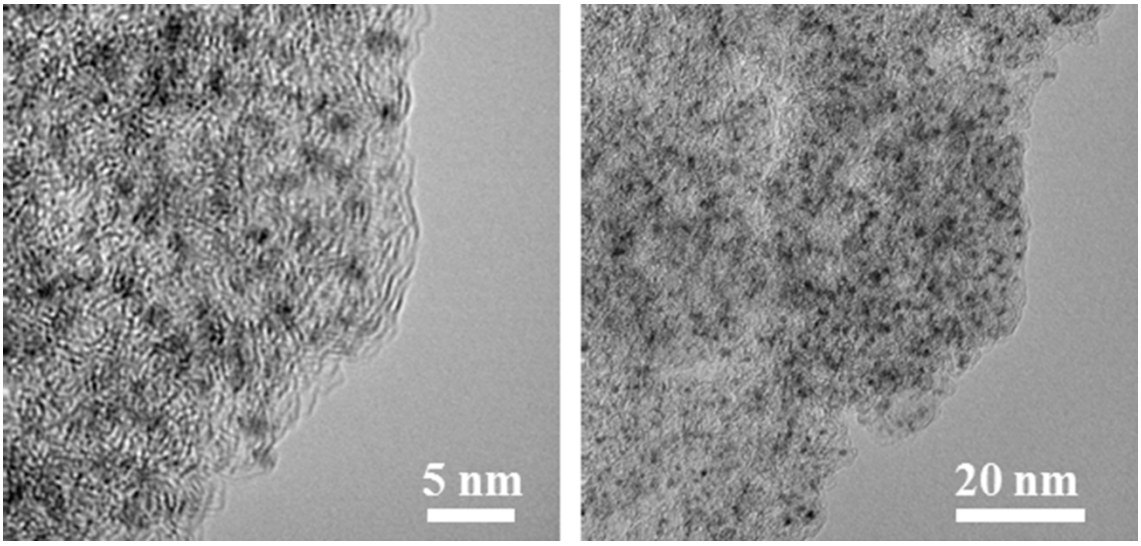

Fig. S3 TEM images of AC/IrIndCOD (10%) after the heat treatment at 400 ºC for 24 h.

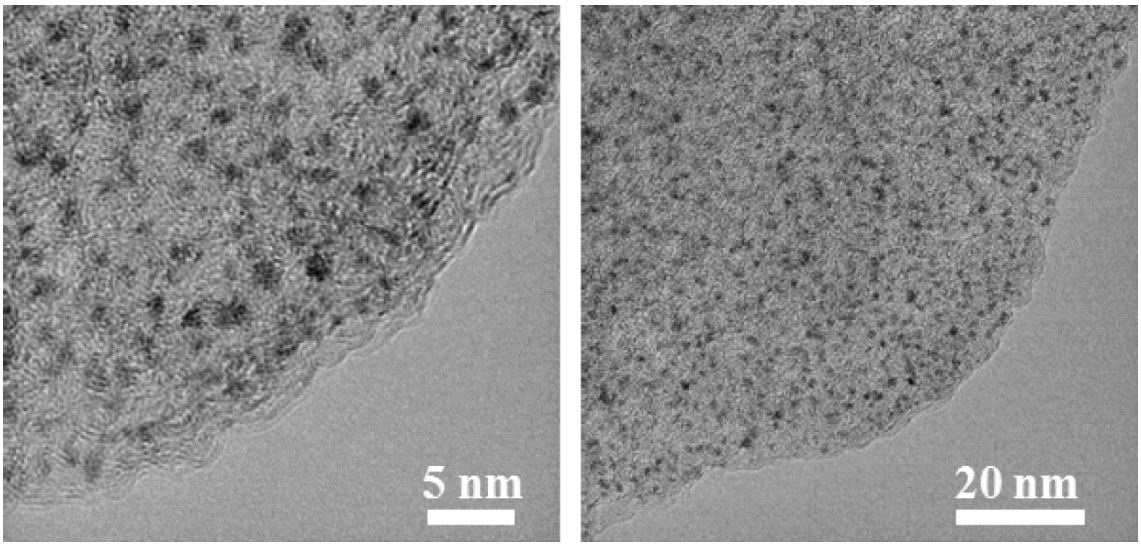

Fig. S4 TEM images of AC/IrIndCOD (10%) after the heat treatment at 500 ºC for 3 h.

Supplementary note 7| Local structures of the AC/Ir samples

Irrespective of the least loading amount among all the AC/Ir samples, AC/Ir (0.5%) has a relatively large amount of Ir nanoparticles by comparing with AC/Ir (10%) (Fig. 3c,d). We then performed the X-ray photoelectron spectroscopy (XPS) analysis for the AC/Ir (0.5%) because we presumed that Ir nanoparticles in AC/Ir (0.5%) preferentially exist near the particle surface of AC. As shown in Fig. S5, the XPS spectrum of AC/Ir (0.5%) exhibited the distinct peaks derived from Ir despite the fact that the Ir loading of AC/Ir (0.5%) is as small as 0.5 wt%. Since Ir nanoparticles were supported within the AC pores, the particle sizes of the supported Ir were controlled below the pore sizes of AC, which was confirmed from the TEM observation (Fig. 3c,d). XPS spectra contain the information of approximately several nanometers deep from the surface. Even if the Ir nanoparticles are not deposited on the particle surface of AC, XPS analysis detects the Ir that exists in the several nanometer deep from the particle surface. Therefore, the result of the XPS measurement suggests that the proportion of Ir nanoparticles existing near the particle surface of AC is relatively high for AC/Ir (0.5%), considering that the AC used in this study has particle sizes from several micrometers to several tens of micrometer (Fig. S6).

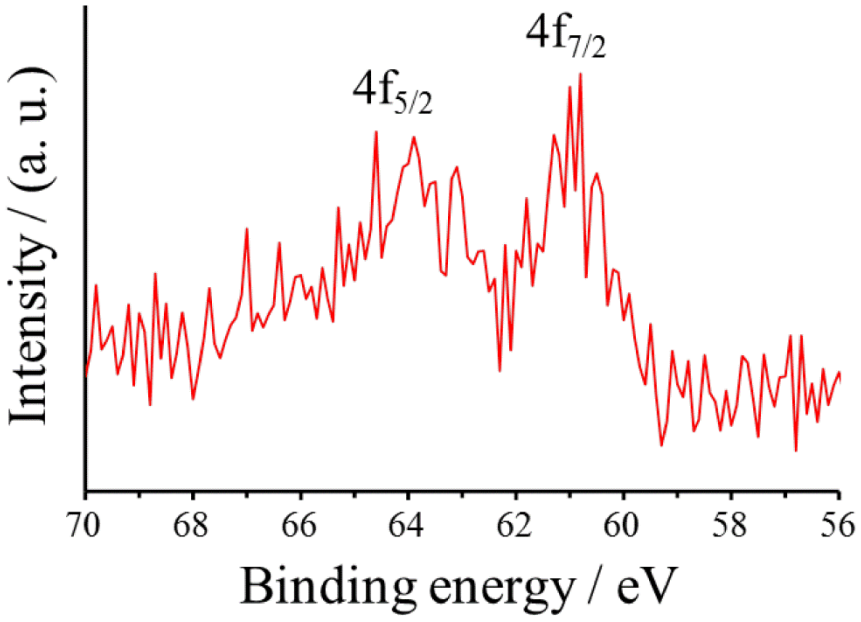

Fig. S5 XPS spectrum of AC/Ir (0.5%).

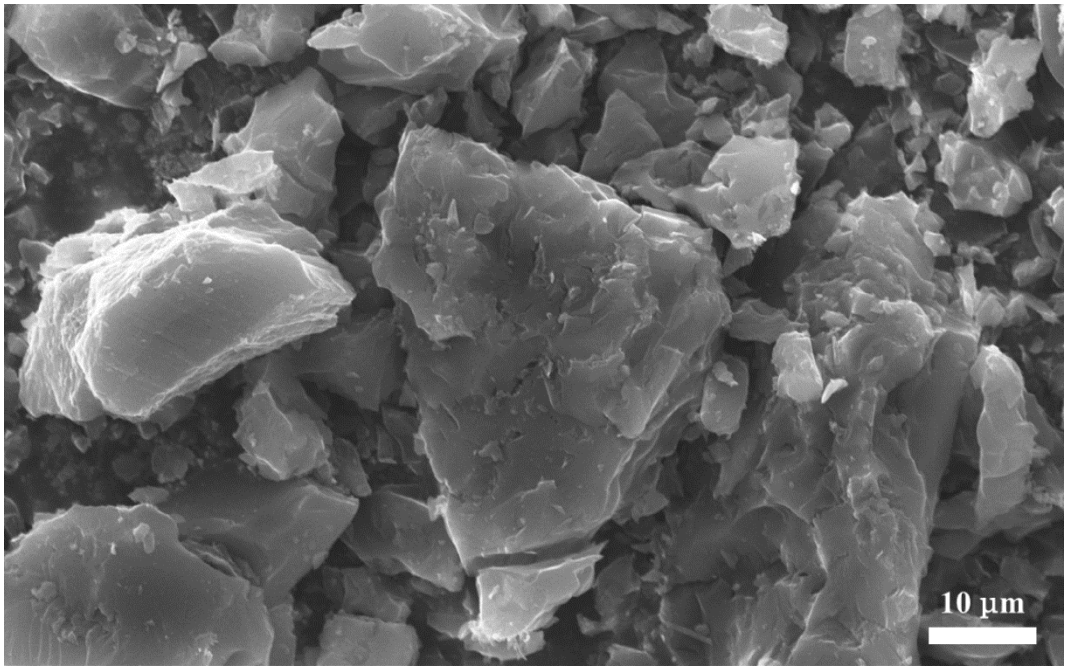

Fig. S6 SEM image of AC.

Once again, we compared the TEM images of AC/Ir (0.5%) with the AC/IrIndCOD (10%) after the heat treatment at 400 ºC for 24 h and 500 ºC for 3 h (Fig. S7a−c). Indeed, the amount of the Ir nanoparticles existing near the particle surface of AC is higher than that in the inner part of the AC particles for AC/Ir (0.5%) (Fig. S7a). In contrast, the Ir nanoparticles in the AC/IrIndCOD (10%) after the heat treatment of 400 ºC for 24 h (Fig. S7b) and 500 ºC for 3 h (Fig. S7c) are uniformly dispersed over the whole AC particles. The difference in the dispersion of Ir nanoparticles can be further confirmed by comparing the TEM images of AC/Ir (0.5%) (Fig. S7d) and the AC/IrIndCOD (10%) after the heat treatment at 500 ºC for 3 h (Fig. S7e).

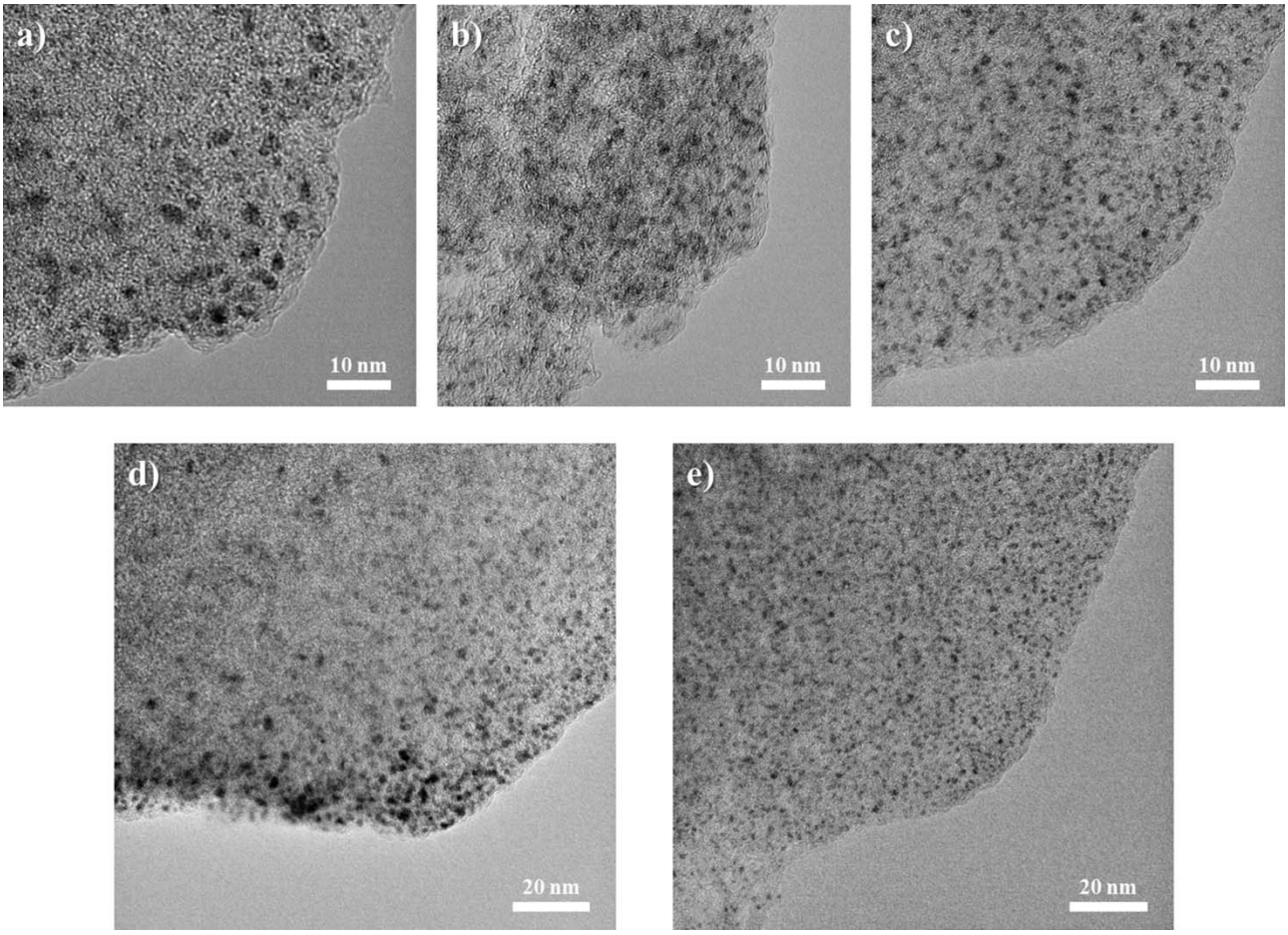

Fig. S7 TEM images of (a,d) AC/Ir (0.5%), (b) AC/IrIndCOD (10%) after the heat treatment at 400 ºC for 24 h, and (c,e) AC/IrIndCOD (10%) after the heat treatment at 500 ºC for 3 h.

References

1. Ravel, B.; Newville, M., ATHENA, ARTEMIS, HEPHAESTUS: data analysis for X-ray absorption spectroscopy using IFEFFIT. *J. Synchrotron Rad.* 2005, ***12***, 537-541.